Gas Phase Characterization of the Noncovalent Quaternary Structure of Cholera Toxin and the Cholera Toxin B Subunit Pentamer

Jonathan P. Williams,* Daniel C. Smith,* Brian N. Green,† Brian D. Marsden,‡ Keith R. Jennings,* Lynne M. Roberts,* and James H. Scrivens*

*Department of Biological Sciences, University of Warwick, Coventry CV4 7AL, United Kingdom; †Waters MS Technologies Centre, Micromass UK Ltd., Manchester M22 5PP, United Kingdom; and ‡Structural Genomics Consortium, University of Oxford, Botnar Research Centre, Oxford OX3 7LD, United Kingdom

ABSTRACT Cholera toxin (CTx) is an AB_5 cytotonic protein that has medical relevance in cholera and as a novel mucosal adjuvant. Here, we report an analysis of the noncovalent homopentameric complex of CTx B chain (CTx B_5) using electrospray ionization triple quadrupole mass spectrometry and tandem mass spectrometry and the analysis of the noncovalent hexameric holotoxin usingelectrospray ionization time-of-flight mass spectrometry over a range of pH values that correlate with those encountered by this toxin after cellular uptake. We show that noncovalent interactions within the toxin assemblies were maintained under both acidic and neutral conditions in the gas phase. However, unlike the related *Escherichia coli* Shiga-like toxin B_5 pentamer (SLTx B), the CTx B_5 pentamer was stable at low pH, indicating that additional interactions must be present within the latter. Structural comparison of the CTx B monomer interface reveals an additional α-helix that is absent in the SLTx B monomer. In silico energy calculations support interactions between this helix and the adjacent monomer. These data provide insight into the apparent stabilization of CTx B relative to SLTx B.

INTRODUCTION

Cholera toxin (CTx), produced by toxinogenic strains of *Vibrio cholerae*, is a heterohexameric AB_5 protein belonging to the family of related toxins that are associated with human disease. Infection with *V. cholerae* can lead to an acute gastrointestinal disease resulting in toxemia and chronic diarrhea causing the loss of over 10–20 liters of body fluids per day in some cases (1) and frequently resulting in a mortality of 20–50% in untreated cases (2,3). Indeed, there are over 200,000 reported new cases of cholera each year (4). CTx, the main toxic product produced during infection, has been characterized, along with the producing bacterium, as a potential 'biowarfare' agent by the US and UK defense agencies (5). The structure of CTx holotoxin and the CTx B pentameric subunits have been determined by means of x-ray crystallography (6–8). These studies revealed that the five B subunits (~11.6 kDa/subunit) form a doughnut-shaped ring and that the A subunit (~27.5 kDa) is composed of two distinct domains, A1 and A2. The A1-domain is responsible for the enzymatic activity of the toxin, whereas the A2-domain assists in the tethering of the A1-domian to the B subunit pentamer by inserting noncovalently into and through the central pore of the B_5 complex (Fig. 1). The CTx A1 subunit is an ADP-ribosyltransferase and NAD-glycohydrolase that can modify G proteins by ADP ribosylation (9). The main intracellular target of CTx directly associated with the induction of fluid secretion is Gs, a G protein involved in the activation of the adenylate cyclase complex (10–12), although the toxin can affect numerous metabolic processes through the modification of other G proteins. Modification of Gs by CTx leads to constitutive activation of the adenylate cyclase complex and elevated intracellular cAMP levels (13–15), which in turn stimulates active chloride secretion (16–18) resulting in a severe form of secretory diarrhea.

To accomplish these intracellular changes, CTx must reach the cytosol of its target cells. CTx binds, via its B pentamer, to the glycosphingolipid GM1 ganglioside (19–21), which is present in the plasma membrane of virtually all cell types, including those cells that line the intestinal tract and certain cells associated with the control and function of the immune system (22). Binding of CTx to GM1 at the plasma membrane triggers toxin uptake and subsequent retrograde delivery of the toxin to the endoplasmic reticulum (ER) (23–28) where the A1-domain is reduced from the A2-B_5 complex and then retrotranslocated across the ER membrane into the target cell cytosol where it can modify its targets (27,29–32).

In addition to the well-characterized cytotonic properties of CTx, interaction between the CTx holotoxin or the isolated B_5 pentamer and specific target cells can also promote signaling pathways not linked to cAMP induction or indeed to other second messenger molecules. This can lead to different immunomodulatory functions, such as mucosal adjuvant effects, depending on the target cell type (22). A key element in the diverse signaling activities of this toxin is the initial oligomerization of GM1 receptors upon binding the B-chain pentamer. This is believed to promote the recruitment of both signaling and accessory molecules into cholesterol-enriched membrane microdomains (lipid rafts) to establish and enhance

Submitted October 20, 2005, and accepted for publication January 19, 2006.

Jonathan P. Williams and Daniel C. Smith contributed equally to this work.

Address reprint requests to Jonathan P. Williams, Dept. of Biological Sciences, University of Warwick, Gibbet Hill Road, Coventry CV4 7AL, UK. Tel.: 44-2476-522157; Fax: 44-2476-523701; E-mail: j.p.williams@warwick.ac.uk.

0006-3495/06/05/3246/09 $2.00

doi: 10.1529/biophysj.105.076455

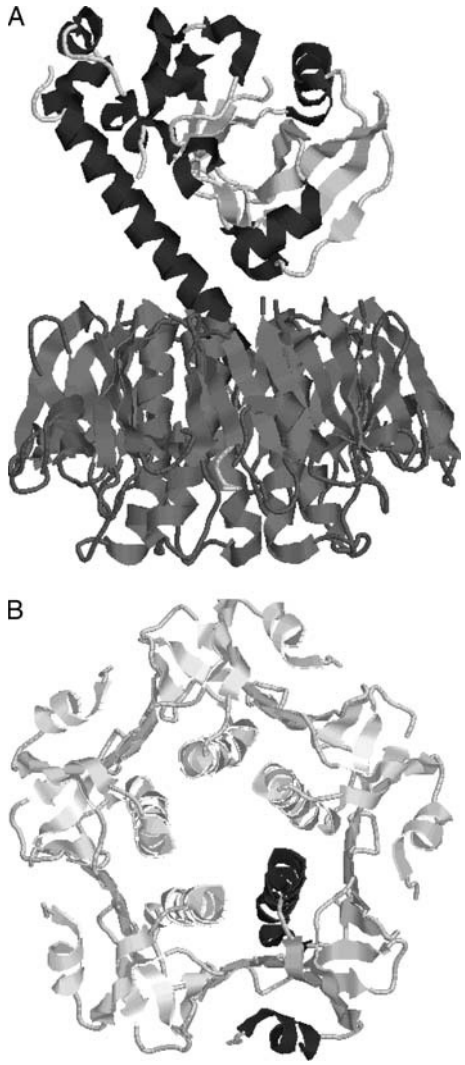

FIGURE 1 Crystal structure of CTx and the CTx B_5 pentamer. (*A*) CTx holotoxin viewed sideways with the surface of the B pentamer that contains the GM1 binding sites facing downward. The catalytic A chain showing secondary structure. The A2 fragment can be seen to insert into the core of the B pentamer. (*B*) CTx B_5 pentamer shown from the top, with a single monomer indicated.

signaling cascades (22,33). As such, analysis of the noncovalent interactions that promote and maintain the quaternary structure of this toxin is of fundamental importance since such interactions have significant biochemical and medical implications.

There have been relatively few reports of the analysis of CTx by mass spectrometry (MS) (34,35). An in-depth study by liquid chromatography MS (LC-MS) and LC tandem MS (LC-MS/MS) provided sequence information derived from tryptic digestion and showed that the toxin was well suited to mass spectrometric detection (35). During this previous investigation, the AB_5 holotoxin was not detected. Here, we demonstrate that the complete noncovalent assembled AB_5 holotoxin remains intact during the electrospray ionization (ESI) process and can be observed in the mass spectrum.

ESI-MS has been shown to be an extremely useful tool in the study of the AB_5 noncovalent assemblies of the Shiga-like toxin (SLTx) and multivalent complexes of SLTx with globotriaoside (36). We have previously shown that SLTx from *Escherichia coli* can be detected over a pH range of 3–7 (37), in contrast to the previous study where the AB_5 holotoxin was not detected at neutral pH (36). Investigation of the dissociation of the homopentamer B_5, B_4, and B_3 assemblies by collision-induced dissociation (CID) in an instrument capable of performing MS/MS experiments was shown to provide dissociation pathways of the assemblies. Information relating to the structure of the assemblies was inferred from the product ions formed from the MS/MS experiments. The results obtained for the dissociation of the homopentamer B_5 during the previous study (37) were consistent with those obtained by thermal decomposition by blackbody infrared radiative dissociation within the cell of a Fourier transform ion cyclotron resonance mass spectrometer (38).

Here, ESI-MS and ESI-MS/MS have been successfully used to examine the noncovalent interactions that exist between the subunits of the complete CTx holotoxin and the pentameric B chains. The first objective of this investigation was to examine the ions produced from the complete hexameric noncovalent holotoxin complex (CTx AB_5). Our results clearly show that the intact complex was observed in the gas phase in a time-of-flight (TOF) mass spectrometer. Furthermore, we report the dissociation of the noncovalent homopentameric binding subunit of the CTx by means of CID in a collision cell of a triple quadrupole mass spectrometer. This has allowed us to probe the noncovalent assembly of CTx and CTx-B5s through their gas phase dissociation pathways.

MATERIALS AND METHODS

CTx and CTx B-subunit were purchased from Sigma (St. Louis, MO). The toxin samples were extensively dialyzed against 10 mM ammonium acetate (Sigma) at pH 7.0, desalted using PD-10 gel filtration columns, and concentrated to a final protein concentration of 16.3 μM for CTx holotoxin and 8.97 μM for CTx B in a Centricon 10 apparatus (Millipore, Watford, UK).

Mass spectrometry

Experiments were performed in a single TOF mass spectrometer (LCT, Waters MS Technologies, Manchester, UK) and a triple quadrupole mass spectrometer (Quattro Ultima, Manchester, UK). In each instrument, noncovalent assemblies were observed by increasing the backing pressure between the source and high vacuum region. Both instruments were equipped with the standard Z-spray ESI source and operated at a source and desolvation temperature of 110°C. Sample solutions were introduced into the source region of the instruments by conventional electrospray, operated in positive mode of ionization with a capillary voltage of 3 kV, and optimized for the transmission of noncovalent assemblies. In the triple quadrupole instrument, tandem mass spectrometry (MS/MS or MS^2) was carried out using argon collision gas at a pressure of 2.5×10^{-3} mbar within the radio-frequency (RF)-only hexapole collision cell.

Data acquisition and processing were carried out using MassLynx (V3.5). Transform or, alternatively, maximum entropy-based software was used to find the masses of the subunits and hence the charges on each multiply

charged ion. All spectra shown were subjected to minimal smoothing. The upper m/z range of the triple quadrupole instrument is 4000 so that, since the monomer has a mass of nearly 11,600, ions of the type B_x^{y+} could be observed only if y is $3x$ or greater.

The complex formed by the homopentameric binding subunit of the CTx (CTx B_5) and the hexameric holotoxin (CTx AB_5) was studied by direct infusion at a concentration of 4.5 pmol/μL and 8 pmol/μL in 10 mM aqueous ammonium acetate at a pH of 4.0–7.0, adjusted by addition of dilute ammonia or formic acid solution, respectively. A Harvard Apparatus (South Natick, MA) Model 22 syringe pump was used to provide a flow rate of 4 μL/min.

Molecular modeling

The structures of SLTx (PDB code 1BOV) and CTx B (PDB code 1FGB) were taken from the Protein Data Bank (PDB) at Brookhaven (39) and imported into the Molsoft ICM program (40). The coordinates of the structures were then converted into internal coordinate space to allow regularization of the structures to be performed. Interchain energy calculations were made using the standard ICM force field (40) between two adjacent monomers (chains A and B in 1BOV and chains D and E in 1FGB). Interactions were specifically analyzed and images made using ICM.

RESULTS AND DISCUSSION

Triple quadrupole MS for the AB_5 holotoxin

Initially, the CTx holotoxin (4 pmol/mL) was analyzed denatured in a solution of acetonitrile/H_2O + 0.2% formic acid. This confirmed the homogeneity of the CTx B components. However, the CTx A protein was heterogeneous and consisted of two components (Fig. 2). Maximum entropy provided the average molecular mass of 11605.2 Da for the CTx B subunit and average molecular masses of 26581.4 Da and 26905.8 Da for the heterogeneous CTx A protein. The maximum entropy deconvoluted spectrum obtained clearly identifies two different major components for the A protein (Fig. 2 *B*).

The A-subunit consists of two chains, A1 (194 residues) and A2 (46 residues) which are connected by a disulphide bridge, whereas the B chain (103 residues) is a single polypeptide (Fig. 3 *A*). The heterogeneity observed within the A chains of these family of proteins is not uncommon, as previously reported for the related AB_5 protein, SLTx (37). The average mass observed at 26905.8 Da for CTx A chain is identical to one observed previously (35) and has been ascribed to the loss of methionine from the N-terminal of the A2 chain together with the loss of two serine residues from the C-terminus of the A1 chain (Fig. 3 *B*). The average mass difference between the observed and predicted mass of 26904.8 Da is 41 parts-per-million (ppm). The peak at 26581.4 Da was not previously observed and probably corresponds to the loss of methionine from the N-terminus of the A2 chain together with the loss of two serine residues, arginine, proline, and alanine from the C-terminus of the A1 chain (Fig. 3 *C*). Again the average mass difference between the observed and predicted mass of 26580.3 Da is 41 ppm. The difference between the predicted and observed mass was extremely low in both cases, conferring a high degree of

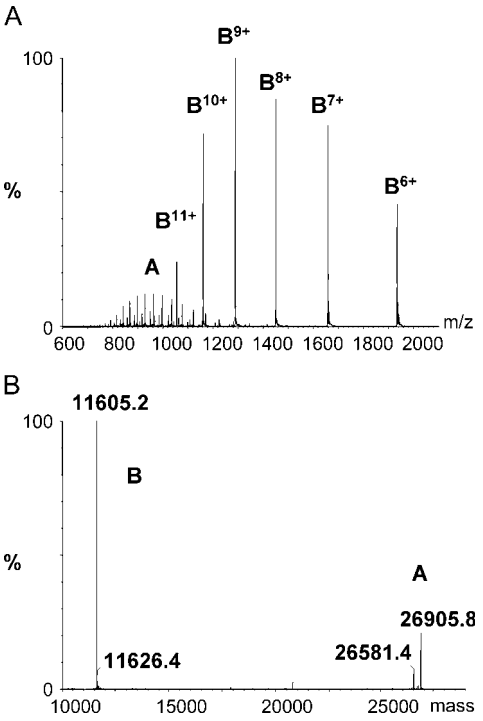

FIGURE 2 ESI-triple quadrupole mass spectrum of the denatured cholera holotoxin at a concentration of 4 pmol/μL in acetonitrile/H_2O + 0.2% formic acid (*A*). Maximum entropy deconvoluted spectrum expanded in the region from m/z 10,000 to 30,000 highlighting the heterogeneity of the A unit (*B*).

confidence in the predicted cleavage patterns. Although the masses agree well with theory, this does not necessarily negate the need to determine the exact sequences for samples in which the origin is not precisely known. However, in this case, the samples were obtained from a commercial source and the full amino acid sequence of the A1, A2, and the B chains is well established (35). It is conceivable that during the periplasmic expression of CTx the A1 and A2 chains are partially trimmed at either or both termini, thus generating

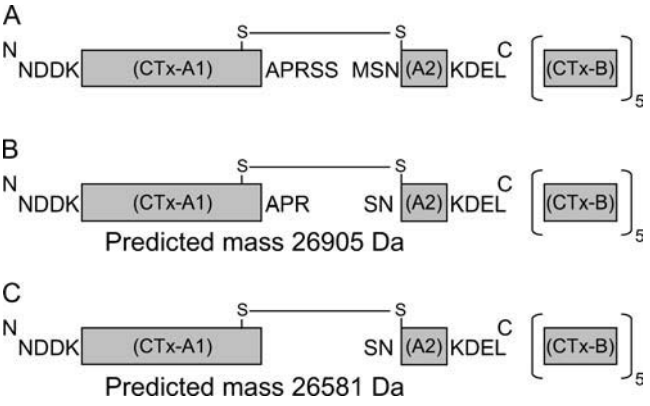

FIGURE 3 Schematic representation of the CTx holotoxin, with the amino acid residues at the amino (N) and carboxyl (C) termini of the A1, A2, and B chains indicated. Shown is the complete CTx holotoxin (*A*), along with the two predicted cleavage products (*B* and *C*).

smaller polypeptide chains, similar to that reported previously for the related SLTx A chain (37).

TOFMS for the AB_5 holotoxin

ESI-TOFMS was used to try to observe the complete noncovalent CTx AB_5 complex in the gas phase. Abundant ions were observed for the B subunit monomer and the B_5 pentamer, with less abundant ions observed for the AB_5 holotoxin ions at pH 7.0 (Fig. 4 *A*). The base peak in the mass spectrum corresponds to the monomer B^{7+}. The partial mass spectrum has been expanded in the region m/z 3000–5000 (Fig. 4 *B*). The abundances of the B_5 pentamer and the AB_5 holotoxin ions remained in fairly constant ratio over the pH range 4.0–7.0 under the condition specified (partial mass spectrum obtained at pH ~ 4.0; Fig. 4 *C*). The abundances of the monomer and pentamer ions observed did not remain constant over the pH range. At pH 5.0 the monomer B^{7+} ion had a relative abundance of ~93% of the base peak corresponding to the pentamer B_5^{17+} ion. At pH 4.0, the monomer B^{7+} ion was observed in the mass spectrum as the base peak and the pentamer B_5^{17+} ion had a relative abundance of ~64% to the monomer B^{7+} ion. The observed charged states for the AB_5 holotoxin extend from 21^+ to 15^+. It is of interest to note that both the AB_5 and B_5 ions were observed throughout the pH range examined, suggesting that the hexameric AB_5 CTx assembly and the pentameric B_5 CTx B assembly were both stable at acidic pH. This is in marked contrast to findings with the structurally related AB_5 SLTx, where the cell-binding B_5 pentamer was less stable at acidic pH than the complete AB_5 holotoxin (37). We therefore suggest that the presence of the A2 portion of CTx A chain is not required to stabilize the CTx B pentamer in the gas phase, as has been postulated for SLTx (37,41,42), but rather that stability arises from the inherent properties of the CTx-B_5. This is consistent with the known stability of CTx B in aqueous solution (6,7,43) where the presence of the A chain had little effect on the stability of the B pentamer.

The heterogeneity of the CTx A chain observed in the triple quadrupole MS was further examined by TOFMS under conditions that maintained the noncovalently associated holotoxin intact in the gas phase. Transformation of the spectrum in the region of m/z 3000–5000, which corresponds to the ions observed for the AB_5 holotoxin, gave suggested molecular mass of 84612.8 Da (calculated 84608.1 Da) and 84932.4 Da (calculated 84932.3 Da) for the heterogeneous AB_5 holotoxin. The results obtained demonstrate that the masses are in good agreement with those expected for the hexameric complex, calculated previously from the denatured complex (Fig. 2).

We have demonstrated that the complete noncovalent assembly of the CTx holotoxin can be detected by ESI-TOFMS over a range of physiological pHs. To our knowledge, this is the first time the CTx holotoxin assembly has been observed intact in the gas phase by MS. The increased sensitivity afforded by TOF mass analyzers for observing

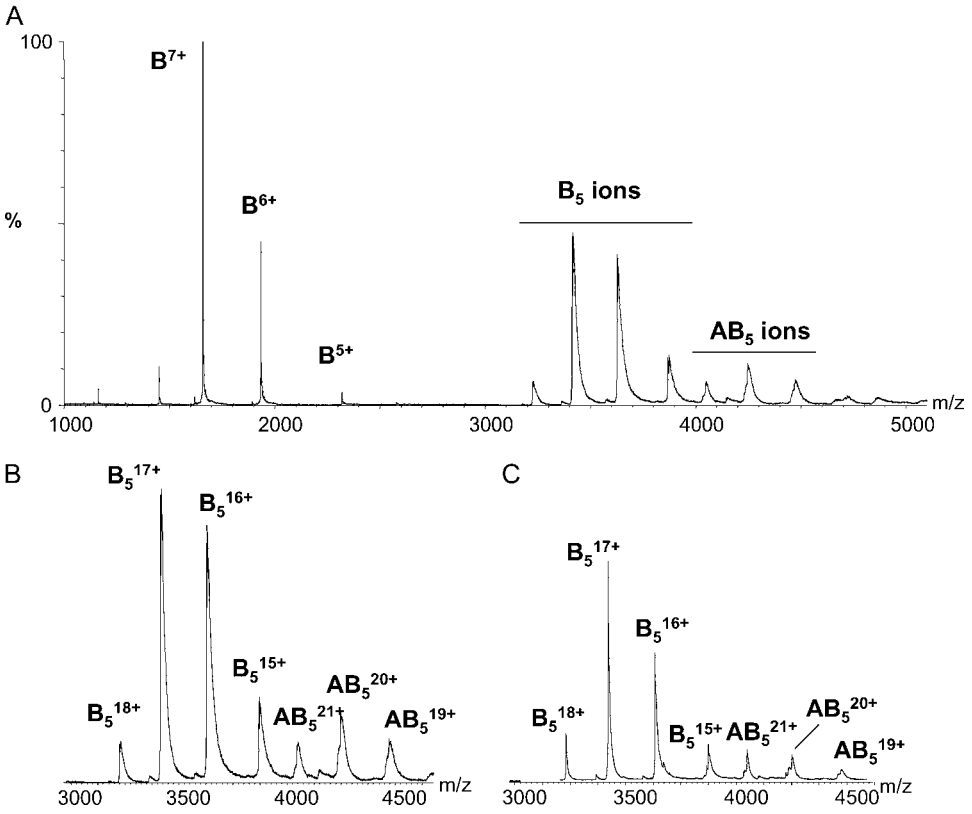

FIGURE 4 ESI-ToF mass spectra obtained for the AB_5 cholera holotoxin buffered with ammonium acetate at pH ~ 7.0 (*A*). Also shown is the noncovalent assembly at pH 7.0 expanded in the region m/z 3000–4500 (*B*) and the noncovalent assembly at pH 4.0 expanded in the region m/z 3000–4500 (*C*).

such AB_5 assemblies intact in the gas phase supports and extends our previous work (37). The high degree of sensitivity also allowed for the accurate detection of differentially trimmed species of the A-chain component of the holotoxin preparation. Over 2 min acquisition time at a flow rate of 4 μL/min, 8 μL of 8 pmol/μL of AB_5 solution was consumed to generate the mass spectra shown.

The TOF instrument is not capable of MS/MS experiments and further investigative studies were performed in a triple quadrupole instrument. The CTx AB_5 ions observed could not be subjected to MS/MS experiments because of the upper mass range of 4000 of the triple quadrupole instrument. Therefore, further MS/MS experiments were carried out solely on the CTx B_5 pentamer.

Triple quadrupole MS for the homopentamer B_5

The CTx pentamer B_5 consists of five identical subunits that arrange into a pentameric ring structure (Fig. 1 *B*). Each subunit has a molecular mass of 11.6 kDa and is composed of 103 amino acids. Initially, the mass spectrum was obtained for the noncovalent complex of CTx B_5 buffered with ammonium acetate at pH ~ 6.6 (Fig. 5). Ions corresponding to the CTx B_5 homopentamer were observed at a range of pH from ~4.0–7.0 (data not shown). The mass spectrum was obtained with a declustering voltage of 60 V. The base peak in the mass spectrum corresponds to B_5^{16+}. The dominant signal corresponds to the intact homopentamer (B_5), with observed charge states extending from 18^+ to 15^+. The pattern of abundance of these ions is identical to the multiply charged species observed with the SLTx B_5 ions, which extended from 15+ to 12+ (37). This presumably reflects the overall similarity in tertiary and quaternary structure between the two toxins. The mass spectrum also shows monomer ions (B) with observed charge states from 8^+ to 5^+. The mass spectrum demonstrates that the homopentamer B_5, the dominant quaternary form of the B subunit protein in solution (44–46), remains intact during the ESI process. Furthermore, the B_5 complex remained intact over a range a pH. Over 3 min acquisition time, at a flow rate of 4 μL/min, 12 μL of 4.5 pmol/μL of B_5 solution was consumed to generate the mass spectra shown.

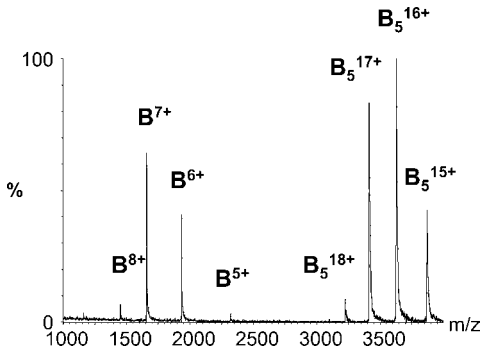

FIGURE 5 ESI-triple quadrupole mass spectrum of the noncovalent complex of CTx-B_5 at pH 6.6.

It has been reported that low pH (~5.0), similar to that found within the endosome compartment of intoxicated target cells, causes a conformational change within the CTx B_5s (47,48). However, this conformational change did not promote bound CTx B to dissociate from the GM1 receptor, but rather caused specific changes that affected the structure of the interface between the protein and the membrane to which CTx B was bound (47). If we presume that under our experimental conditions CTx B undergoes a similar structural alteration, we would not predict a destabilization of the B_5 pentameric assembly in the gas phase. Given that the GM1 binding site, as revealed by the crystal structure, is formed between two adjacent monomers, our data are completely consistent with this, insofar as low pH does not alter the binding of CTx to GM1 (47) or, as reported here, does not destabilize the noncovalent CTx B-pentamer.

Triple quadrupole MS/MS of the homopentamer B_5

MS/MS was then used to investigate the dissociation pathway of the homopentamer B_5^{17+} ion (Fig. 6). The two dominant ions in the mass spectrum of the homopentamer correspond to B_5^{16+} and B_5^{17+} (Fig. 5). The B_5^{17+} ion was selected as a precursor ion to undergo CID in the collision cell of the

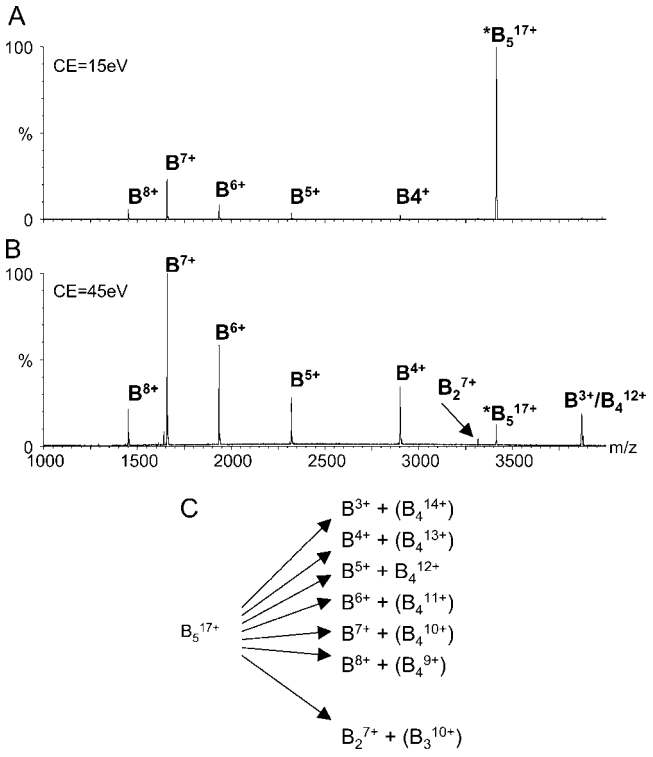

FIGURE 6 ESI-Triple quadrupole MS/MS mass spectra of the noncovalent complex of CT-B_5. Shown is the dissociation obtained at a collision energy of 15 eV (*A*) and 45 eV (*B*) for the precursor ion B_5^{17+}. Shown is the possible dissociation pathway for the B_5^{17+} ion (*C*).

instrument, the collision energy being varied (15–45 eV (E_{LAB} = 255–765 eV)) to obtain intense fragment ions (product ions). An increase in the abundance of product ions was observed as the collision energy was increased (Fig. 6 *B*). The multiply protonated pentamer species B_5^{17+} selected for CID dissociates almost entirely via the loss of one subunit (Fig. 6 *B*) to form primarily abundant monomer ions having a range of charges. A very low abundant dimer B_2^{7+} ion is also observed. The B_5^{17+} dissociation formed monomer, dimer, trimer, and tetramer ions, but no peaks which could be unequivocally assigned to trimer ions were observed. These ions could still be formed, however, as the ions B_3^{3+}, B_3^{6+}, and B_3^{9+} cannot be distinguished from the ions B^{+}, B^{2+}, and B^{3+}, B_2^{2+}, B_2^{4+}, and B_2^{6+}, and B_4^{4+}, B_4^{8+}, and B_4^{12+}, respectively, to which some of the peaks have been assigned. However, not all of the ions that are predicted to form were detected (Fig. 6 *C*). This was either due to them being present in very low abundance or due to the m/z ratio of the ion being beyond the upper m/z range of the instrument, 4000, as discussed above. This is important since the pentamer ion selected for dissociation does not only form monomer ions with a range of charges, it must form tetramer ions with a range of charges also. The tetramer ions formed though, for example B_4^{10+}, will unfortunately not be detected due to the limited m/z range of the instrument.

The dissociation of 50% of the CTx precursor ion B_5^{17+} required a collision energy of 40 eV, (E_{LAB} 680 eV) ~2.4-fold higher than that seen for the SLTx precursor ions B_5^{14+} (Fig. 7) and B_5^{13+} (37), which both showed 50% dissociation of the precursor ions at ~20 eV (E_{LAB} 280 eV).

A rough comparison of the relative stability of the two complexes may be gained from a comparison of the relative collision energies required to reduce the intensities of the two precursor ions, B_5^{17+} (CTx) and B_5^{14+} (SLTx), to 50% of their initial abundances at similar collision gas pressures. An exact comparison cannot be made since the ions carry different numbers of charges and the distribution of products is unknown in each case. For the CTx complex, a 50% reduction in the abundance of the B_5^{17+} ion was observed when a potential difference of 40 V was applied between the source and the RF-only collision cell, corresponding to a laboratory collision energy, E_{LAB}, of $17 \times 40 = 680$ eV. For the SLTx complex, a similar reduction in the abundance of the B_5^{14+} ion was observed with a potential difference of 20 V, corresponding to a laboratory collision energy, E_{LAB}, of $14 \times 20 = 280$ eV. The approximate masses of the two complexes are 58 kDa and 38 kDa, respectively, and the collision gas was argon, mass 40 Da. The amount of energy available to effect dissociation, the center-of-mass collision energy E_{COM}, is given by $E_{COM} = E_{LAB} \times (m_{Ar}/(m_{Ar} + m_{ion})) \times 96.5$ kJ mol^{-1}, where E_{LAB} is the ion kinetic energy in the laboratory frame of reference, m_{Ar} is the mass of argon the collision cell gas, and m_{ion} is the mass of the precursor ion. This leads to values of ~45 kJ mol^{-1} and 28 kJ mol^{-1} for the CTx and SLTx complexes, respectively, implying that ~1.5 times as much energy is required to effect the dissociation of the CTx pentamer compared to the SLTx B complex.

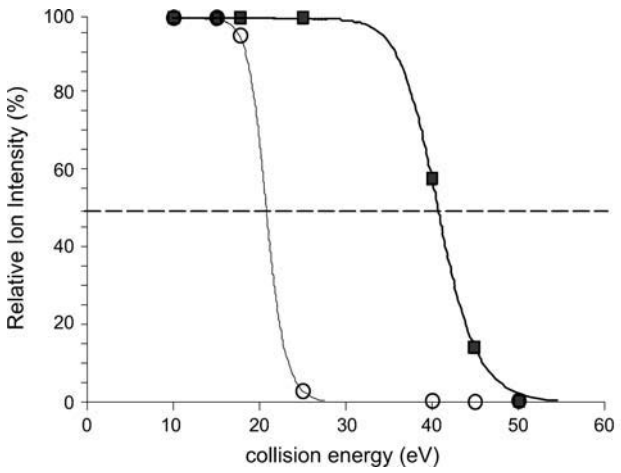

FIGURE 7 Plot of the relative ion intensity for the SLTx B_5^{+14} ion (*open symbols*) and the CTx B_5^{+17} ion (*solid symbols*) versus the collision energy (eV) applied to the ions. The amplitudes of the energy of the two curves at 50% of the intensity provide a measure of the relative gas phase stability of the complexes.

This difference in pentamer stability is also seen in aqueous solution (44,46,49). Despite these differences, a high degree of structural stability exists in both the CTx and SLTx B_5 pentamers at physiological pH (37). This has been attributed to the large number of intersubunit interactions that occur between monomers (6,50). The amount of surface area buried during pentamer assembly differs between the two toxins, with CTx B having a greater buried surface area (2700 A^2) than SLTx B (>1269 A^2 < 2700 A^2) (6,51). The degree of buried surface area correlates well with the measured stabilities of the two pentamers (44), implying that additional interactions must be present within the CTx B monomer-monomer interface to account for its increased stability. We therefore compared the monomer interface region in the two different pentameric proteins. This revealed that the CTx B monomer interface has an additional α-helix which lies in front of the continuous β-sheet that forms the majority of the CTx B monomer interactions (Fig. 8 *A*) and this region of secondary structure contains residues that interact with residues that lie in the adjacent monomer. The SLTx B monomer interface region, however, possesses only the continuous β-sheet structure and not the α-helix (Fig. 8 *B*). In silico energy calculations were performed using the crystal structures of the CTx B (PDB code 1FGB) and SLTx B (PBD code 1BOV) pentamers to assess the theoretical interactions that exist between the additional helix present in the CTx B structure that can interact with the adjacent monomer (Table 1). The comparison of the pentameric structures provides an insight into the apparent stabilization of CTx B relative to SLTx B. The additional N-terminal helix shown in the CTx B structure is involved in a number of extra interactions between monomers such that the intermonomer

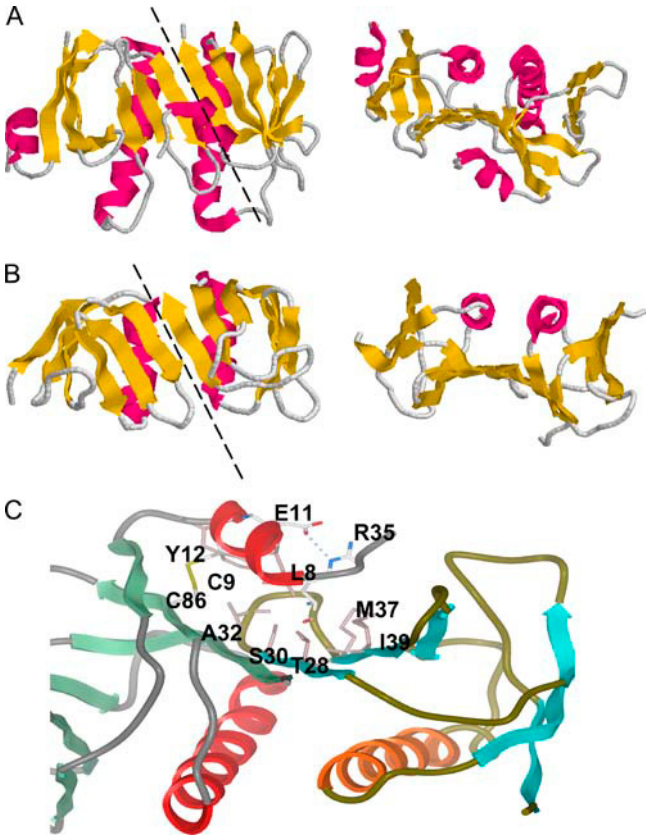

FIGURE 8 Crystal structures of adjacent monomers within the CTx B and SLTx B pentamers. Monomers from CTx B (*A*) and SLTx B (*B*) viewed either sideways (*left*) showing the interface region (*dashed line*) between monomers or from the top (*right*) of the molecule. Structures colored to indicate secondary structure (α-helix in *red* and β-sheet in *yellow*). Proposed intermonomer interactions present in CTx B. The chain on the left is chain E; the one on the right is chain D. Chain E is colored differently from D to distinguish between the two. The critical residues in the intermonomer interactions are picked out. E11/R35 are shown in standard atomic colors. Residues involved in hydrophobic interactions are colored pink. The hydrogen bond between E11 and R35 is shown, as is the disulphide bridge. Image was made using ICM.

interaction energy is ~2.4 times greater than between the monomers of SLTx B. This value is in agreement with that determined experimentally for the increase in energy required to dissociate the two complexes. This revealed that the additional interactions in the CTx B pentamer would most likely result in an increased degree of stability of ~236 kJ mol^{-1} to this molecule compared to the SLTx B pentamer. Although the gas phase experimentally determined values are much lower than the theoretically calculated values of 405.7 and 169.5 kJ mol^{-1}, respectively, for monomer-monomer interactions (Table 1), this is to be expected because of the contribution of coulombic repulsion in the fragmenting of the highly charged complexes. The gas phase stability calculation assumes that a single collision has occurred to the precursor ion; however as is the case for large complexes studied here, to reduce the precursor ion intensity by 50%, multiple collisions will occur and contribute to the E_{COM} value. As gas phase complexes

TABLE 1 Monomer-monomer interaction energies for the CTx B and SLTx B pentamers*

Protein	Bond†	Bond energy‡	Protein	Bond	Bond energy
CTx B	vdw	−230.3	SLTx B	vdw	−123.9
(1fgb)	hb	−76.6	(1bov)	hb	−5.4
	el	−98.8		el	−40.2
	total§	−405.7 (−236.2)¶		total	−169.5
		Gas phase stability‖			Gas phase stability
CTx B		45.1 (17.0)**	SLTx B		28.1

*Intersubunit interactions calculated from the x-ray structures (PDB codes) and experimental gas phase dissociation data.
†Bond type: vdw; van der Waals contact contribution (i.e., hydrophobic); hb, hydrogen bond contribution; and el, electrostatic contribution (but not including H-bond).
‡Bond energy calculated using Molsoft ICM program (kJ mol^{-1}).
§Total calculated energies associated with the monomer-monomer interactions.
¶Calculated energy difference between CTx B and SLTx B.
‖Experimental energy derived from the center of mass collision energy (kJ mol^{-1}).
**Experimental energy difference between CTx B and SLTx B.

are desolvated before mass analysis, the hydrogen bonding and electrostatic interactions that survive ESI are possibly accountable for maintaining the quaternary structure of the desolvated complexes, whereas the hydrophobic interactions may be lost or partially lost in the gas phase. As such, complete correlation of gas phase and solution phase binding energies would not be expected. Rather, the experimental and theoretical results above show a similar trend, implying that the dominant interactions stabilizing the quaternary structure are maintained in the gas phase and can provide a rough comparison to those in solution. The overwhelming majority of the difference in energy can be accounted for by the presence of a strong hydrogen-bond interaction between E11 in the first monomer with R35 in the second (Fig. 8 *C*). Also there is a significant area of hydrophobic contact between the N-terminal underside of the additional helix and the top of the nearby sheet from the neighboring monomer (Fig. 8 *C*). It is important to note that the N-terminal α-helix is held in place by an intramolecular disulphide bridge (C9–C86), which therefore helps to maintain a nonplastic surface for the monomers to interact. We propose that although the interface regions between adjacent monomers has a larger surface area in the CTx B pentamer, the additional interactions present in the CTx B helical region (residues 1–14) may provide the increase in structural stability observed in both the gas and aqueous phase. To further investigate these structural differences in the gas phase, a more detailed comparative study is now required between different B_5 pentamers.

CONCLUSIONS

As with all types of gas phase experiments, care must be taken in the interpretation of the data, as normally the proteins

studied reside and function within an aqueous environment. We believe that the data obtained in this study, however, are highly relevant and informative, particularly since the pH conditions used were near-physiological. As in our previous study (37), data were obtained over a range of pH conditions that correlates well with those encountered by the toxin within the intestinal lumen during infection by *V. cholerae*. Data for both the CTx AB_5 holotoxin and the B_5 pentamer have demonstrated that the noncovalent interactions within the toxin assemblies are maintained, and observable, under both acidic and neutral conditions in the gas phase. Furthermore, unlike the SLTx B_5 pentamer, the CTx B_5 pentamer is stable at acidic pH, indicating that although the two related pentamers share a similar fold at their β-sheet monomer-monomer interfaces (50), additional interactions must be present within the CTx B pentamer to account for its increased stability. Since the initial stages of CTx mediated cellular signaling are dependent on receptor oligomerization after binding of the pentameric B chains, a rapid, sensitive technique to examine the quaternary structure of both native and any genetically engineered protein variants of CTx will be beneficial to further research performed on this toxin.

We thank Prof. Robert Freedman and Dr. Catherine Marsden for critical reading, helpful discussion, and advice with the manuscript.

This study was supported by a Wellcome Trust program grant (063058/Z/00/Z) to L.M.R.

REFERENCES

1. Black, R. E. 1993. Epidemiology of diarrhoeal disease: implications for control by vaccines. *Vaccine*. 11:100–106.
2. Thiagarajah, J. R., and A. S. Verkman. 2005. New drug targets for cholera therapy. *Trends Pharmacol. Sci*. 26:172–175.
3. Sack, D. A., R. B. Sack, G. B. Nair, and A. K. Siddique. 2004. Cholera. *Lancet*. 363:223–233.
4. World Health Organization. 2003. Cholera. *Wkly. Epidemiol. Rec*. 78: 269–276.
5. United Nations. 1993. Convention on the prohibition of the development, production, stockpiling and use of chemical weapons and on their destruction. Paris, France.
6. Zhang, R. G., M. L. Westbrook, E. M. Westbrook, D. L. Scott, Z. Otwinowski, P. R. Maulik, R. A. Reed, and G. G. Shipley. 1995. The 2.4 Å crystal structure of cholera toxin B subunit pentamer: choleragenoid. *J. Mol. Biol*. 251:550–562.
7. Zhang, R. G., D. L. Scott, M. L. Westbrook, S. Nance, B. D. Spangler, G. G. Shipley, and E. M. Westbrook. 1995. The three-dimensional crystal structure of cholera toxin. *J. Mol. Biol*. 251:563–573.
8. Merritt, E. A., P. Kuhn, S. Sarfaty, J. L. Erbe, R. K. Holmes, and W. G. Hol. 1998. The 1.25 Å resolution refinement of the cholera toxin B-pentamer: evidence of peptide backbone strain at the receptor-binding site. *J. Mol. Biol*. 282:1043–1059.
9. De Haan, L., and T. R. Hirst. 2004. Cholera toxin: a paradigm for multi-functional engagement of cellular mechanisms (Review). *Mol. Membr. Biol*. 21:77–92.
10. Sharp, G. W., and S. Hynie. 1971. Stimulation of intestinal adenyl cyclase by cholera toxin. *Nature*. 229:266–269.
11. Guerrant, R. L., L. C. Chen, and G. W. Sharp. 1972. Intestinal adenylcyclase activity in canine cholera: correlation with fluid accumulation. *J. Infect. Dis*. 125:377–381.
12. Johnson, G. L., H. R. Kaslow, and H. R. Bourne. 1978. Genetic evidence that cholera toxin substrates are regulatory components of adenylate cyclase. *J. Biol. Chem*. 253:7120–7123.
13. Field, M., D. Fromm, Q. al-Awqati, and W. B. Greenough. 1972. Effect of cholera enterotoxin on ion transport across isolated ileal mucosa. *J. Clin. Invest*. 51:796–804.
14. Schafer, D. E., W. D. Lust, J. B. Polson, J. Hedtke, B. Sircar, A. K. Thakur, and N. D. Goldberg. 1971. The possible role of cyclic AMP in some actions of cholera toxin. *Ann. N. Y. Acad. Sci*. 185:376–385.
15. Schafer, D. E., W. D. Lust, B. Sircar, and N. D. Goldberg. 1970. Elevated concentration of adenosine 3′:5′-cyclic monophosphate in intestinal mucosa after treatment with cholera toxin. *Proc. Natl. Acad. Sci. USA*. 67:851–856.
16. Field, M., M. C. Rao, and E. B. Chang. 1989. Intestinal electrolyte transport and diarrheal disease (2). *N. Engl. J. Med*. 321:879–883.
17. Cheng, S. H., D. P. Rich, J. Marshall, R. J. Gregory, M. J. Welsh, and A. E. Smith. 1991. Phosphorylation of the R domain by cAMP-dependent protein kinase regulates the CFTR chloride channel. *Cell*. 66:1027–1036.
18. Burch, R. M., C. Jelsema, and J. Axelrod. 1988. Cholera toxin and pertussis toxin stimulate prostaglandin E2 synthesis in a murine macrophage cell line. *J. Pharmacol. Exp. Ther*. 244:765–773.
19. Heyningen, S. V. 1974. Cholera toxin: interaction of subunits with ganglioside GM1. *Science*. 183:656–657.
20. Griffiths, S. L., R. A. Finkelstein, and D. R. Critchley. 1986. Characterization of the receptor for cholera toxin and *Escherichia coli* heat-labile toxin in rabbit intestinal brush borders. *Biochem. J*. 238:313–322.
21. Schengrund, C. L., and N. J. Ringler. 1989. Binding of *Vibrio* cholera toxin and the heat-labile enterotoxin of *Escherichia coli* to GM1, derivatives of GM1, and nonlipid oligosaccharide polyvalent ligands. *J. Biol. Chem*. 264:13233–13237.
22. Smith, D. C., J. M. Lord, L. M. Roberts, and L. Johannes. 2004. Glycosphingolipids as toxin receptors. *Semin. Cell Dev. Biol*. 15:397–408.
23. Sandvig, K., B. Spilsberg, S. U. Lauvrak, M. L. Torgersen, T. G. Iversen, and B. van Deurs. 2004. Pathways followed by protein toxins into cells. *Int. J. Med. Microbiol*. 293:483–490.
24. Massol, R. H., J. E. Larsen, Y. Fujinaga, W. I. Lencer, and T. Kirchhausen. 2004. Cholera toxin toxicity does not require functional Arf6- and dynamin-dependent endocytic pathways. *Mol. Biol. Cell*. 15: 3631–3641.
25. Lencer, W. I. 2004. Retrograde transport of cholera toxin into the ER of host cells. *Int. J. Med. Microbiol*. 293:491–494.
26. Feng, Y., A. P. Jadhav, C. Rodighiero, Y. Fujinaga, T. Kirchhausen, and W. I. Lencer. 2004. Retrograde transport of cholera toxin from the plasma membrane to the endoplasmic reticulum requires the trans-Golgi network but not the Golgi apparatus in Exo2-treated cells. *EMBO Rep*. 5:596–601.
27. Lencer, W. I., and B. Tsai. 2003. The intracellular voyage of cholera toxin: going retro. *Trends Biochem. Sci*. 28:639–645.
28. Fujinaga, Y., A. A. Wolf, C. Rodighiero, H. Wheeler, B. Tsai, L. Allen, M. G. Jobling, T. Rapoport, R. K. Holmes, and W. I. Lencer. 2003. Gangliosides that associate with lipid rafts mediate transport of cholera and related toxins from the plasma membrane to endoplasmic reticulum. *Mol. Biol. Cell*. 14:4783–4793.
29. Teter, K., M. G. Jobling, and R. K. Holmes. 2003. A class of mutant CHO cells resistant to cholera toxin rapidly degrades the catalytic polypeptide of cholera toxin and exhibits increased endoplasmic reticulum-associated degradation. *Traffic*. 4:232–242.
30. Tsai, B., C. Rodighiero, W. I. Lencer, and T. A. Rapoport. 2001. Protein disulfide isomerase acts as a redox-dependent chaperone to unfold cholera toxin. *Cell*. 104:937–948.
31. Tsai, B., and T. A. Rapoport. 2002. Unfolded cholera toxin is transferred to the ER membrane and released from protein disulfide isomerase upon oxidation by Ero1. *J. Cell Biol*. 159:207–216.
32. Tsai, B., Y. Ye, and T. A. Rapoport. 2002. Retro-translocation of proteins from the endoplasmic reticulum into the cytosol. *Nat. Rev. Mol. Cell Biol*. 3:246–255.

33. Hirst, T. R., S. Fraser, M. Soriani, A. T. Aman, H. L. de Haan, A. Hearn, and E. Merritt. 2002. New insights into the structure-function relationships and therapeutic applications of cholera-like enterotoxins. *Int. J. Med. Microbiol.* 291:531–535.

34. Takao, T., H. Watanabe, and Y. Shimonishi. 1985. Facile identification of protein sequences by mass spectrometry. B subunit of *Vibrio cholerae* classical biotype Inaba 569B toxin. *Eur. J. Biochem.* 146:503–508.

35. van Baar, B. L., A. G. Hulst, and E. R. Wils. 1999. Characterisation of cholera toxin by liquid chromatography—electrospray mass spectrometry. *Toxicon.* 37:85–108.

36. Kitova, E. N., P. I. Kitov, D. R. Bundle, and J. S. Klassen. 2001. The observation of multivalent complexes of Shiga-like toxin with globotriaoside and the determination of their stoichiometry by nanoelectrospray Fourier-transform ion cyclotron resonance mass spectrometry. *Glycobiology.* 11:605–611.

37. Williams, J. P., B. N. Green, D. C. Smith, K. R. Jennings, K. A. Moore, S. E. Slade, L. M. Roberts, and J. H. Scrivens. 2005. Noncovalent Shiga-like toxin assemblies: characterization by means of mass spectrometry and tandem mass spectrometry. *Biochemistry.* 44:8282–8290.

38. Felitsyn, N., E. N. Kitova, and J. S. Klassen. 2001. Thermal decomposition of a gaseous multiprotein complex studied by blackbody infrared radiative dissociation. Investigating the origin of the asymmetric dissociation behavior. *Anal. Chem.* 73:4647–4661.

39. Berman, H. M., J. Westbrook, Z. Feng, G. Gilliland, T. N. Bhat, H. Weissig, I. N. Shindyalov, and P. E. Bourne. 2000. The protein data bank. *Nucleic Acids Res.* 28:235–242.

40. Abagyan, R. A., M. M. Totrov, and D. A. Kuznetsov. 1994. ICM—a new method for protein modeling and design: applications to docking and structure prediction from the distorted native conformation. *J. Comput. Chem.* 15:488–506.

41. Jemal, C., J. E. Haddad, D. Begum, and M. P. Jackson. 1995. Analysis of Shiga toxin subunit association by using hybrid A polypeptides and site-specific mutagenesis. *J. Bacteriol.* 177:3128–3132.

42. Fraser, M. E., M. M. Chernaia, Y. V. Kozlov, and M. N. James. 1994. Crystal structure of the holotoxin from Shigella dysenteriae at 2.5 Å resolution. *Nat. Struct. Biol.* 1:59–64.

43. van Heyningen, S. U. 1982. Conformational changes in subunit A of cholera toxin following the binding of ganglioside to subunit B. *Eur. J. Biochem.* 122:333–337.

44. Goins, B., and E. Freire. 1988. Thermal stability and intersubunit interactions of cholera toxin in solution and in association with its cell-surface receptor ganglioside GM1. *Biochemistry.* 27:2046–2052.

45. Surewicz, W. K., J. J. Leddy, and H. H. Mantsch. 1990. Structure, stability, and receptor interaction of cholera toxin as studied by Fourier-transform infrared spectroscopy. *Biochemistry.* 29:8106–8111.

46. Pina, D. G., and L. Johannes. 2005. Cholera and Shiga toxin B-subunits: thermodynamic and structural considerations for function and biomedical applications. *Toxicon.* 45:389–393.

47. McCann, J. A., J. A. Mertz, J. Czworkowski, and W. D. Picking. 1997. Conformational changes in cholera toxin B subunit-ganglioside GM1 complexes are elicited by environmental pH and evoke changes in membrane structure. *Biochemistry.* 36:9169–9178.

48. Picking, W. L., H. Moon, H. Wu, and W. D. Picking. 1995. Fluorescence analysis of the interaction between ganglioside GM1-containing phospholipid vesicles and the B subunit of cholera toxin. *Biochim. Biophys. Acta.* 1247:65–73.

49. Pina, D. G., J. Gomez, E. Villar, L. Johannes, and V. L. Shnyrov. 2003. Thermodynamic analysis of the structural stability of the Shiga toxin B-subunit. *Biochemistry.* 42:9498–9506.

50. Sixma, T. K., P. E. Stein, W. G. Hol, and R. J. Read. 1993. Comparison of the B-pentamers of heat-labile enterotoxin and verotoxin-1: two structures with remarkable similarity and dissimilarity. *Biochemistry.* 32:191–198.

51. Stein, P. E., A. Boodhoo, G. J. Tyrrell, J. L. Brunton, and R. J. Read. 1992. Crystal structure of the cell-binding B oligomer of verotoxin-1 from *E. coli*. *Nature.* 355:748–750.